







Acidic extracellular pH drives accumulation of N1-acetylspermidine and recruitment of protumor neutrophils

Miki Kato ^{a,1}, Keisuke Maeda^{a,1}, Ryuichi Nakahara^{a,b,1}, Haruka Hirose^{c,d}, Ayano Kondo^e, Sho Aki^{a,b}, Maki Sugaya^a, Sana Hibino ^f, Miyuki Nishida^a, Manami Hasegawa^a, Hinano Morita ^g, Ritsuko Ando^a, Rika Tsuchida^a, Minoru Yoshida ^h, Tatsuhiko Kodama^a, Hideyuki Yanai ^f, Teppei Shimamura^{c,d} and Tsuyoshi Osawa ^{a,b,*}

^aDivision of Nutriomics and Oncology, RCAST, The University of Tokyo, Tokyo 153-8904, Japan

^bDepartment of Chemistry and Biotechnology, Graduate School of Engineering, The University of Tokyo, Tokyo 113-0033, Japan

^cDepartment of Systems Biology, Graduate School of Medicine, Nagoya University, Nagoya 466-8550, Japan

^dDepartment of Computational and Systems Biology, Medical Research Institute, Tokyo Medical and Dental University, Tokyo 113-8510, Japan

^eResearch Unit, R&D Division, Kyowa Kirin Co., Ltd., Tokyo 100-0004, Japan

^fDepartment of Inflammolgy, RCAST, The University of Tokyo, Tokyo 153-8904, Japan

^gCollege of Natural Sciences, University of Texas at Austin, Austin, TX 78712, USA

^hChemical Genomics Research Group, RIKEN Center for Sustainable Resource Science, Saitama 351-0198, Japan

*To whom correspondence should be addressed: Email: osawa@lsbm.org

¹M.K., K.M., and R.N. contributed equally to this work.

Edited By: J. Silvio Gutkind

Abstract

An acidic tumor microenvironment plays a critical role in tumor progression. However, understanding of metabolic reprogramming of tumors in response to acidic extracellular pH has remained elusive. Using comprehensive metabolomic analyses, we demonstrated that acidic extracellular pH (pH 6.8) leads to the accumulation of N1-acetylspermidine, a protumor metabolite, through up-regulation of the expression of spermidine/spermine acetyltransferase 1 (SAT1). Inhibition of SAT1 expression suppressed the accumulation of intra- and extracellular N1-acetylspermidine at acidic pH. Conversely, overexpression of SAT1 increased intra- and extracellular N1-acetylspermidine levels, supporting the proposal that SAT1 is responsible for accumulation of N1-acetylspermidine. While inhibition of SAT1 expression only had a minor effect on cancer cell growth in vitro, SAT1 knockdown significantly decreased tumor growth in vivo, supporting a contribution of the SAT1-N1-acetylspermidine axis to protumor immunity. Immune cell profiling revealed that inhibition of SAT1 expression decreased neutrophil recruitment to the tumor, resulting in impaired angiogenesis and tumor growth. We showed that antineutrophil-neutralizing antibodies suppressed growth in control tumors to a similar extent to that seen in SAT1 knockdown tumors in vivo. Further, a SAT1 signature was found to be correlated with poor patient prognosis. Our findings demonstrate that extracellular acidity stimulates recruitment of protumor neutrophils via the SAT1-N1-acetylspermidine axis, which may represent a metabolic target for antitumor immune therapy.

Keywords: cancer metabolism, acidic extracellular pH, N1-acetylspermidine, SAT1, neutrophils

Significance Statement

Acidic tumor microenvironments appear to play a critical role in tumor progression. Recent work has identified several genetic and epigenetic transformations of cancer in response to acidic pH, but an understanding of tumor metabolic reprogramming at acidic pH has been lacking. We used comprehensive nontarget and quantitative metabolomic analyses to show that acidic extracellular pH has a unique metabolic signature linked to protumorigenic immunity. Acidic extracellular pH stimulates the SAT1-N-acetylspermidine axis and activates protumor neutrophils. The results shown here serve as a foundation for development of future therapeutics against aggressive cancer cells in acidic tumor microenvironments, with an ability to improve conventional cancer therapy in combination with immunomodulation.

Introduction

Metabolic reprogramming of cancer is an essential alteration for tumor progression, enhancing drug resistance, tumor invasion, and metastasis (1, 2). Aerobic and anaerobic glycolysis are

representative metabolic reprogramming processes in cancer (described as the Warburg and Pasteur effects, respectively) (3, 4) and occur concomitant with tumor acidosis (5). We and others have reported that acidic microenvironments stimulate fat mass and

Competing Interest: No potential conflict of interest was reported by the authors.

Received: March 30, 2023. **Accepted:** September 11, 2023

© The Author(s) 2023. Published by Oxford University Press on behalf of National Academy of Sciences. This is an Open Access article distributed under the terms of the Creative Commons Attribution-NonCommercial-NoDerivs licence (<https://creativecommons.org/licenses/by-nc-nd/4.0/>), which permits non-commercial reproduction and distribution of the work, in any medium, provided the original work is not altered or transformed in any way, and that the work is properly cited. For commercial re-use, please contact journals.permissions@oup.com

obesity-associated (FTO) genes and sterol regulatory element-binding protein 2 (SREBP2)-induced lipid metabolism to promote tumor progression (6). However, an understanding of metabolic reprogramming and interactions of cancer cells with fibroblasts and immune cells in acidic, as distinct from hypoxic or nutrient-limited, tumor microenvironments, remain elusive.

The polyamine pathway is stimulated in highly metastatic cancers such as castration-resistant prostate cancer (7), colon cancer (8), medulloblastoma (9), and v-raf murine sarcoma (SARC) viral oncogene homolog B1 (BRAF)-mutant melanoma (10). Polyamine metabolites may stimulate cancer-associated fibroblasts (11) and promote antitumor immunity (12), but the mechanism by which polyamine-associated metabolic reprogramming triggers aggressive cancers and its role in tumor progression remains largely unknown.

Accumulation of protumorigenic metabolites plays an important role in tumor progression by stimulating noncanonical metabolic flux (13). For example, 2-hydroxyglutarate is a well-known oncometabolite that supports cancer cell proliferation and is frequently associated with isocitrate dehydrogenase 1/2 (*IDH1/2*) mutations that allow escape from the canonical tricarboxylic acid (TCA) cycle in leukemia and brain tumors, particularly under hypoxia (14–16). Another escape from the canonical TCA cycle is mediated by cancer-associated metabolites such as succinate and fumarate (17). We previously reported a protumor metabolite, phosphoethanolamine, present under glutamine deficiency, that escapes the phospholipid biosynthetic pathway and promotes tumor persistence (18). Although a number of oncometabolites have been reported (19–21), few have been characterized in an acidic tumor microenvironment.

Here, we aimed to employ comprehensive nontarget and quantitative metabolomics to identify protumor metabolites present at acidic pH and identify potential molecular pathways involved in protumorigenic immunomodulation under these conditions.

Results

Acidic pH–altered polyamine metabolism in cancer cells is a metabolic alteration distinct from those in hypoxia and nutrient starvation

Acidic pH is a typical characteristic of the microenvironment of malignant cancers; however, metabolic reprogramming of cancer cells in this context is largely unknown. To investigate the metabolic reprogramming of cancer cells in an acidic environment, we established an acidic culture system to maintain cancer cells at pH 6.8 (Fig. 1A) (6). A comprehensive nontargeted metabolomic analysis of pancreatic cancer (PANC-1) cells using capillary electrophoresis–mass spectrometry (CE-MS) revealed that more than 100 metabolites, including N1-acetylspermidine, were significantly altered in cancer cells under conditions of extracellular acidity (Fig. 1B; Table S1). To further examine whether an acidic environment induces metabolic alterations that are distinct from those of hypoxia and nutrient starvation, we conducted quantitative metabolomic analyses on pancreatic cancer cells (PANC-1 and AsPC-1) cultured under hypoxic, nutrient-starved, or acidic conditions, all of which are common traits in the tumor microenvironment. Then, we compared the data with those cultured under control condition.

Acidic pH specifically altered 159 metabolites, including 79 metabolites present at higher levels and 80 metabolites present at lower levels in PANC-1 cells, along with 56 metabolites present at higher levels and 60 metabolites present at lower levels in AsPC-1 cells (Fig. 1C and D; Fig. S1A and B and Table S1). These changes were distinct from those characteristics of hypoxia or

nutrient starvation in pancreatic cancer cells (Fig. 1C and D; Fig. S1A and B and Tables S2 and S3), suggesting that acidic pH-induced metabolic pathways are distinct from those of hypoxia and nutrient starvation.

Next, we examined which metabolic pathways are enriched in acidic environments. Pathway analysis for metabolites present at higher levels under acidic conditions revealed that the urea cycle and glycolytic pathways (Warburg effect) were up-regulated in PANC-1 and AsPC-1 cells, similar to results seen under hypoxia (Fig. 1E; Fig. S1C). In contrast, glycerophospholipid metabolism and nucleobase catabolism were found to be involved in metabolic reprogramming under nutrient starvation (Fig. 1E; Fig. S1C). These data suggest that acidic extracellular environment and hypoxia induce similar metabolic pathways that are distinct from those induced by nutrient starvation, as previously reported (18).

To further investigate specific metabolic reprogramming induced by acidic pH, we focused on metabolites that were altered only in the acidic environment. We found accumulation of N1-acetylspermidine under acidic conditions, along with down-regulation of putrescine and spermidine in the polyamine pathway in a broad array of various human cancer cells (PANC-1, AsPC-1, HeLa, A431, and HCT116) (Fig. 1F; Fig. S2A and B), suggesting that the acidic pH-induced alteration in polyamine pathway is a general metabolic signature conserved in human cancer cells. This alteration was not observed under hypoxia or nutrient starvation in PANC-1, AsPC-1, and HeLa cells (Tables S1–S3). We next quantified metabolites in other polyamine-related pathways such as the urea cycle and methionine salvage pathways at pH 6.8 in human cancer cells (PANC-1, AsPC-1, HeLa, A431, and HCT116) and compared the results to those obtained at pH 7.4 (Fig. S2C). However, metabolites in the methionine pathway and urea cycle pathways did not accumulate in cancer cells under acidic pH. We also confirmed that lactic acidosis (pH 6.8) also led to accumulation of N1-acetylspermidine in cancer cells (Fig. S2D). Based on these results, we hypothesized that accumulation of N1-acetylspermidine plays a role in acidic pH-induced tumor progression.

SAT1 is responsible for N1-acetylspermidine accumulation

To elucidate a key enzymatic regulator for the accumulation of N1-acetylspermidine, we measured the mRNA expression and protein levels of enzymes in polyamine pathway at acidic pH (pH 6.8) as compared to control condition (pH 7.4) (Fig. 2A). We found that spermidine/spermine acetyltransferase 1 (SAT1), a rate-limiting enzyme of the polyamine pathway, was up-regulated by acidic pH in a series of human cancer cells (PANC-1, AsPC-1, HeLa, A431, and HCT116 cells) at both the mRNA (Fig. 2B; Fig. S3A) and protein levels (Fig. 2C; Fig. S3B), suggesting that acidic pH-induced SAT up-regulation is conserved in human cancer cells. In addition, other rate-limiting enzymes such as SRM and PAOX were down-regulated at the mRNA level (Fig. 2B; Fig. S3A) but not altered at the protein level at acidic pH (Fig. 2C; Fig. S3B). We also examined whether enzymes in the urea and methionine pathways may have been altered to stimulate the polyamine pathway; however, the enzymes in these pathways were not altered at acidic pH, other than arginosuccinate lyase (ASL) (Fig. S3C), suggesting that SAT1 is a key enzyme for N1-acetylspermidine accumulation.

To test whether SAT1 was responsible for N1-acetylspermidine accumulation, we knocked down SAT1 using siRNAs (Fig. 2D; Fig. S4A and B). siRNA-mediated silencing of SAT1 under acidic conditions impaired the accumulation of both intracellular and

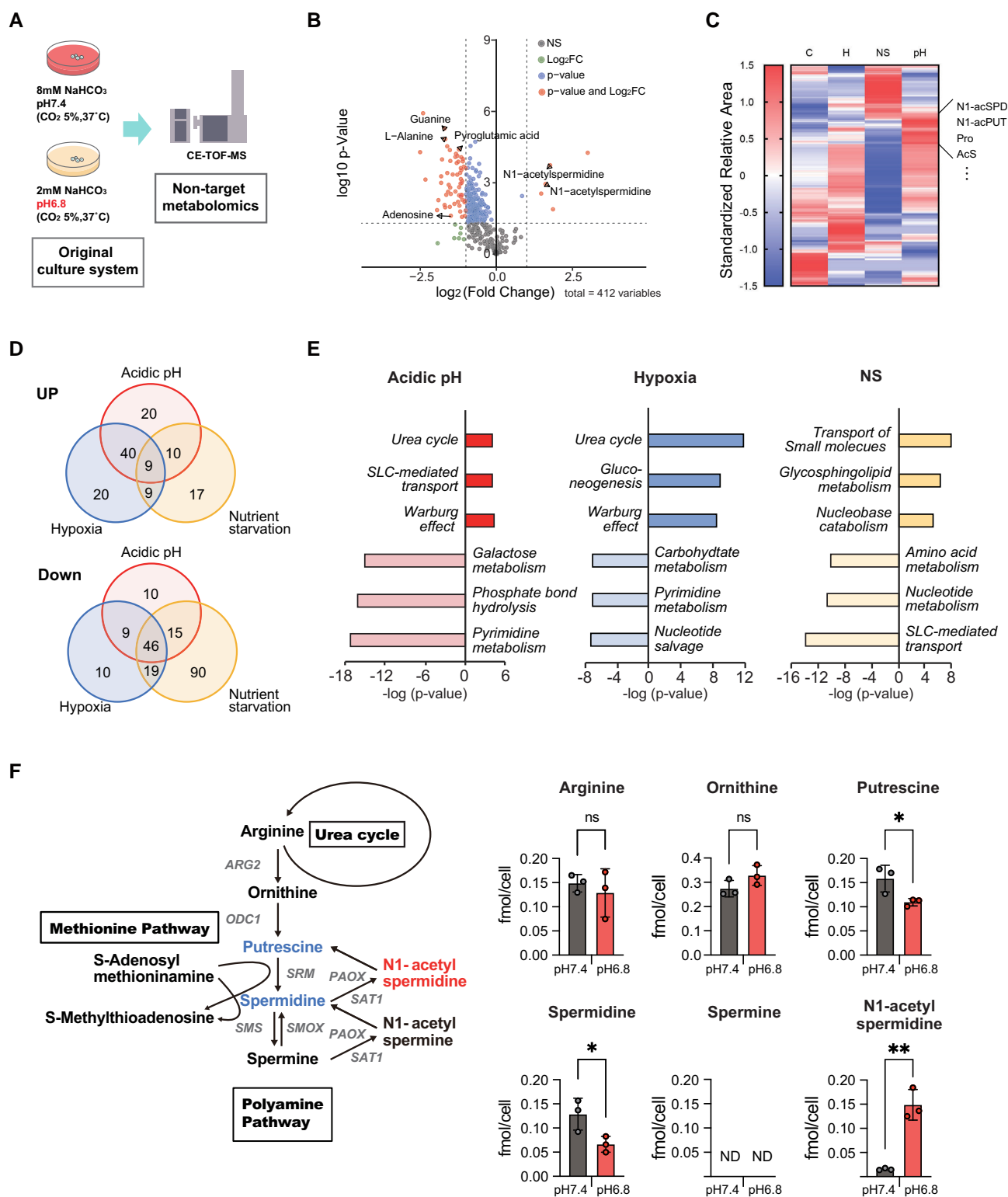


Fig. 1. Targeted and nontargeted metabolomic analyses reveal up-regulation of polyamine metabolism under acidic culture conditions. A) Schematic of experimental design illustrating acidic culture system and nontargeted metabolomics. Cancer cells were cultured under control (pH 7.4) or acidic (pH 6.8) culture conditions for 24 h, and then intracellular metabolites were extracted and subjected to targeted or nontargeted metabolomic analysis using CE-TOFMS. B) Nontargeted metabolomics revealing differential intracellular metabolomic profiles in PANC-1 cells between control (pH 7.4) and acidic (pH 6.8) conditions. Metabolites significantly up- or down-regulated under acidic conditions were fold change more than 1.5 and P-value less than 0.05, and other metabolites were defined as not significantly changed. C) Heatmap representation of differential intracellular metabolomic profiles in PANC-1 cells under control (C), acidic (pH), hypoxic (H), or nutrient starvation (NS) conditions. Representative targeted metabolites specifically up- or down-regulated at low pH are listed. D) Venn diagram showing the numbers of metabolites in PANC-1 cells up- or down-regulated at least 1.5-fold under acidic, hypoxic, or nutrient starvation conditions. E) Pathway analysis of metabolites up- or down-regulated at least two-fold in PANC-1 cells under acidic, hypoxic, or nutrient starvation conditions. F) Schematic of polyamine pathway. Metabolites up- or down-regulated under acidic conditions are shown in red or blue, respectively (left). Intracellular levels of polyamine pathway metabolites in PANC-1 cells under control (pH 7.4) or acidic (pH 6.8) conditions (right). Data represent the mean \pm SEM of at least three independent experiments. NS: not significant; * $P < 0.05$; ** $P < 0.01$.

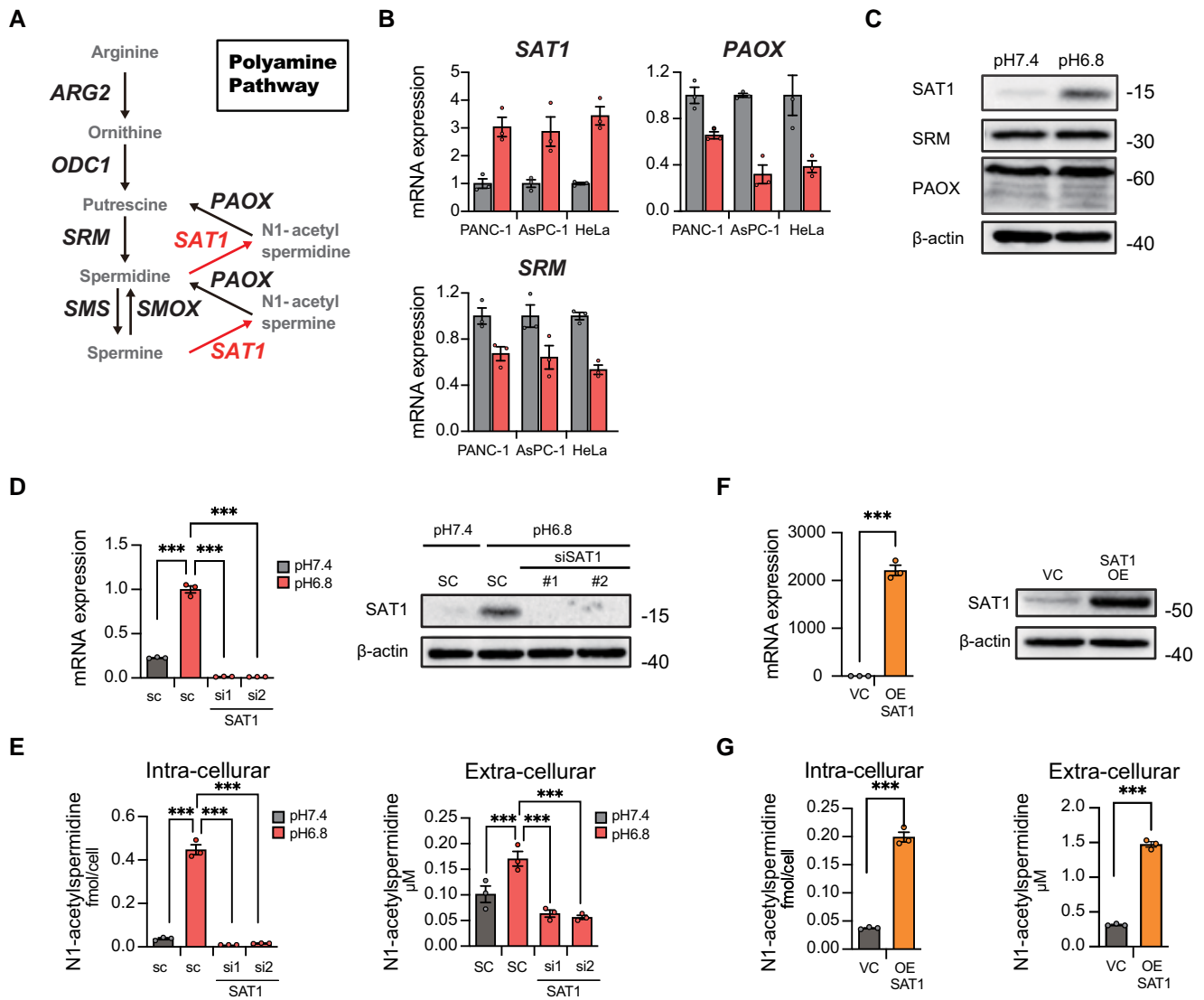


Fig. 2. SAT1 up-regulation is responsible for N1-acetylspermidine accumulation. A) Schematic of polyamine pathways showing enzymes for each step. SAT1 catalyzes conversion of spermine and spermidine to N1-acetylspermine and N1-acetylspermidine, respectively. B) mRNA expression of SAT1, SRM, and PAOX, late limiting enzymes in cancer cells under control (pH 7.4) or acidic (pH 6.8) conditions. C) Protein expression of SAT1, SRM, PAOX, and actin in PANC-1 cells under control (pH 7.4) or acidic (pH 6.8) conditions. D) Validation of SAT1 siRNA-mediated silencing by qPCR and western blotting in PANC-1 cells under control (pH 7.4) or acidic (pH 6.8) conditions. E) Intracellular and extracellular levels of N1-acetylspermidine in PANC-1 with and without silencing of SAT1 under control (pH 7.4) or acidic (pH 6.8) conditions. F) Validation of SAT1 overexpression in PANC-1 cells. G) Intracellular and extracellular levels of N1-acetylspermidine in PANC-1 cells with and without overexpression of SAT1. Data represent the mean \pm SEM of at least three independent experiments. NS: not significant; * $P < 0.05$; ** $P < 0.01$; *** $P < 0.001$.

extracellular N1-acetylspermidine in PANC-1 and HeLa cells (Fig. 2E; Fig. S4C). Moreover, SAT1 overexpression increased the accumulation of N1-acetylspermidine in PANC-1 and HeLa both intracellularly and extracellularly at pH 7.4 (Fig. 2F and G; Fig. S4D–F). In addition, disruption of SAT1 expression (silencing/overexpression of SAT1) did not affect the levels of other metabolites, including putrescine, spermidine, and spermine (not detected [N.D.]), in the polyamine pathway (Fig. S4C and F), supporting the hypothesis that SAT1 is responsible for the accumulation of N1-acetylspermidine at acidic pH.

Inhibition of SAT1 expression suppresses tumor growth through decreased recruitment of immune cells and angiogenesis

To examine the role of SAT1 in tumor progression, we silenced SAT1 in PANC-1 and HeLa cells and examined in vitro and in

vivo cell growth. Although silencing of SAT1 had only a minor effect on cell proliferation in vitro (Fig. S5A), constitutive silencing of SAT1 using shRNA significantly suppressed tumor growth for HeLa and PANC-1 cells in vivo, associated with decreased N1-acetylspermidine levels (Fig. 3A–C; Fig. S5B and C), suggesting a role for the SAT1–N1-acetylspermidine axis in immunomodulation of tumorigenesis. To explore the role of SAT1 in tumorigenicity, we examined whether SAT1 influences the recruitment of CD11b⁺ myeloid cells into tumors. SAT1 knockdown significantly suppressed CD11b⁺ myeloid cell infiltration and decreased angiogenesis (Fig. 3C). To further investigate the role of SAT1 in the recruitment of immune cells, RNA-seq analysis was conducted on SAT1 knockdown tumor samples, and the results were compared with those for shRNA control tumors. Gene expression analysis revealed that inhibition of SAT1 expression decreased leukocyte activation and leukocyte-mediated immunity (Fig. 3D and E), whereas the senescence-associated secretory

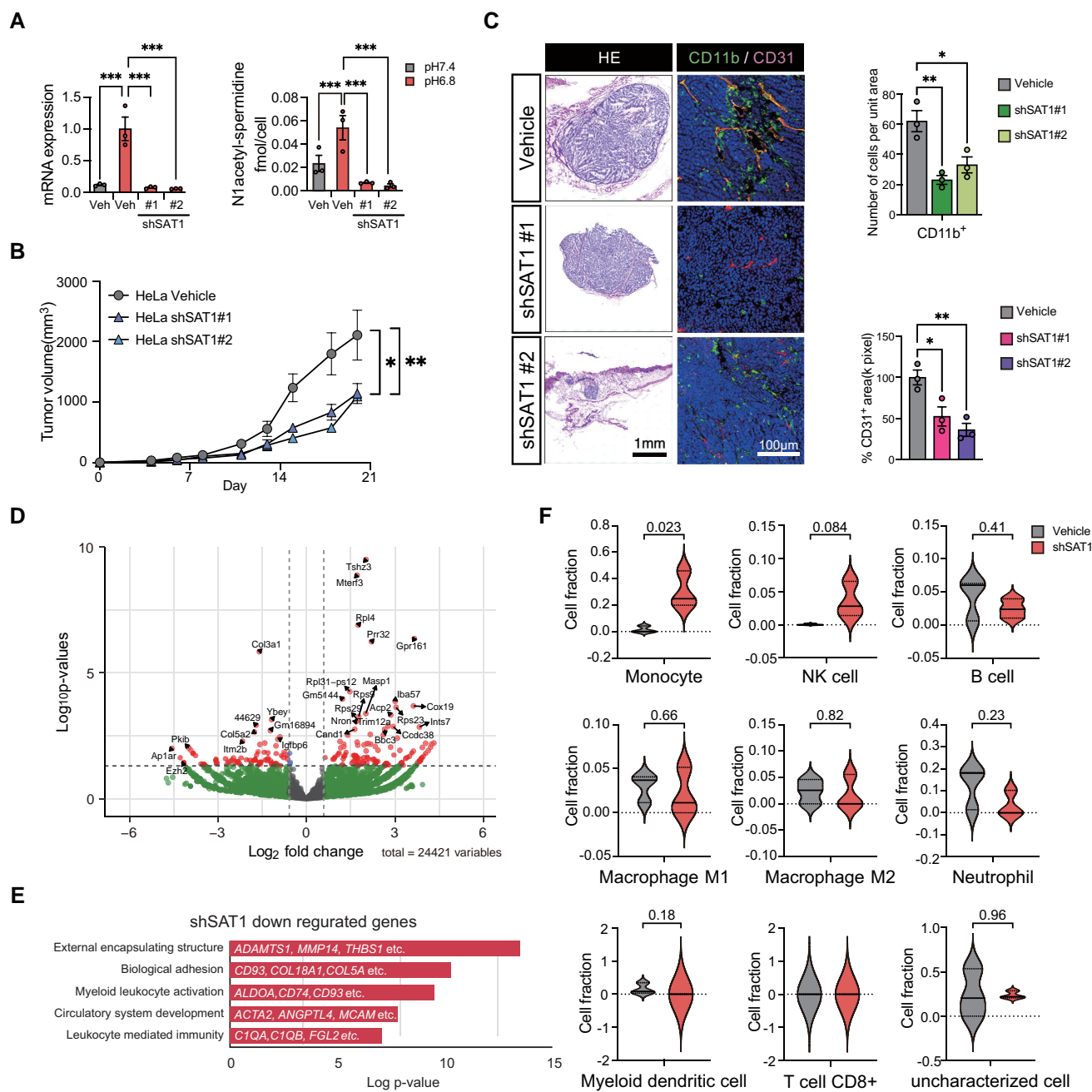


Fig. 3. Inhibition of SAT1 expression suppresses tumor growth through decreased angiogenesis and recruitment of immune cells (leukocytes). **A**) Validation of SAT1 shRNA-mediated silencing and intracellular levels of N1-acetylspermidine in HeLa cells with and without shRNA-mediated silencing of SAT1 under control (pH 7.4) or acidic (pH 6.8) conditions. **B**) Tumor growth curve of HeLa xenografts with and without shRNA-mediated silencing of SAT1. **C**) Hematoxylin and eosin staining and immunostaining of HeLa xenografts with and without shRNA-mediated silencing of SAT1. Myeloid cells, endothelial cells, and nuclei were detected using CD11b, CD31 and DAPI, respectively. Scale bars: 1 mm (left). Numbers of CD11b⁺ myeloid cells per unit area and percentage of CD31⁺ area in tumor xenograft. Scale bars: 100 μm (right). **D**) RNA-seq of HeLa xenograft tissue showing differentially expressed host (fibroblasts/immune cells)-derived genes regulated by shRNA-mediated silencing of SAT1. **E**) Pathway analysis of host (fibroblasts/immune cells)-derived genes up-regulated at least two-fold in tumor tissue by shRNA-mediated silencing of SAT1 in HeLa xenografts. **F**) Immune profiling of SAT1 knockdown tumor tissue. Violin plots of the differences in percentage of cell types identified by quanTIseq in shSAT1 and control samples. Data represent the mean ± SEM of at least three independent experiments. NS: not significant; *P < 0.05; **P < 0.01; ***P < 0.001.

phenotype (SASP) pathway was enriched in cancer cells (Fig. S5D and E). Immune profiling of SAT1 knockdown tumor tissue using quanTIseq suggested that the fraction of monocytes and NK cells increased while the fraction of neutrophils and M1 and M2 macrophages decreased in shSAT1 knockdown tumors (Fig. 3F). Taken together, the results indicate that SAT1 modulates tumor immunity and angiogenesis during tumor progression.

SAT1-mediated recruitment of neutrophils stimulates tumor progression

Since SAT1 may affect immunomodulation, we assessed whether inhibition of SAT1 expression in cancer cells suppressed infiltration of immune cells into tumors. Inhibition of SAT1 expression increased natural killer (NK) cell and dendritic cell numbers and suppressed infiltration of neutrophils into tumors (Fig. 4A),

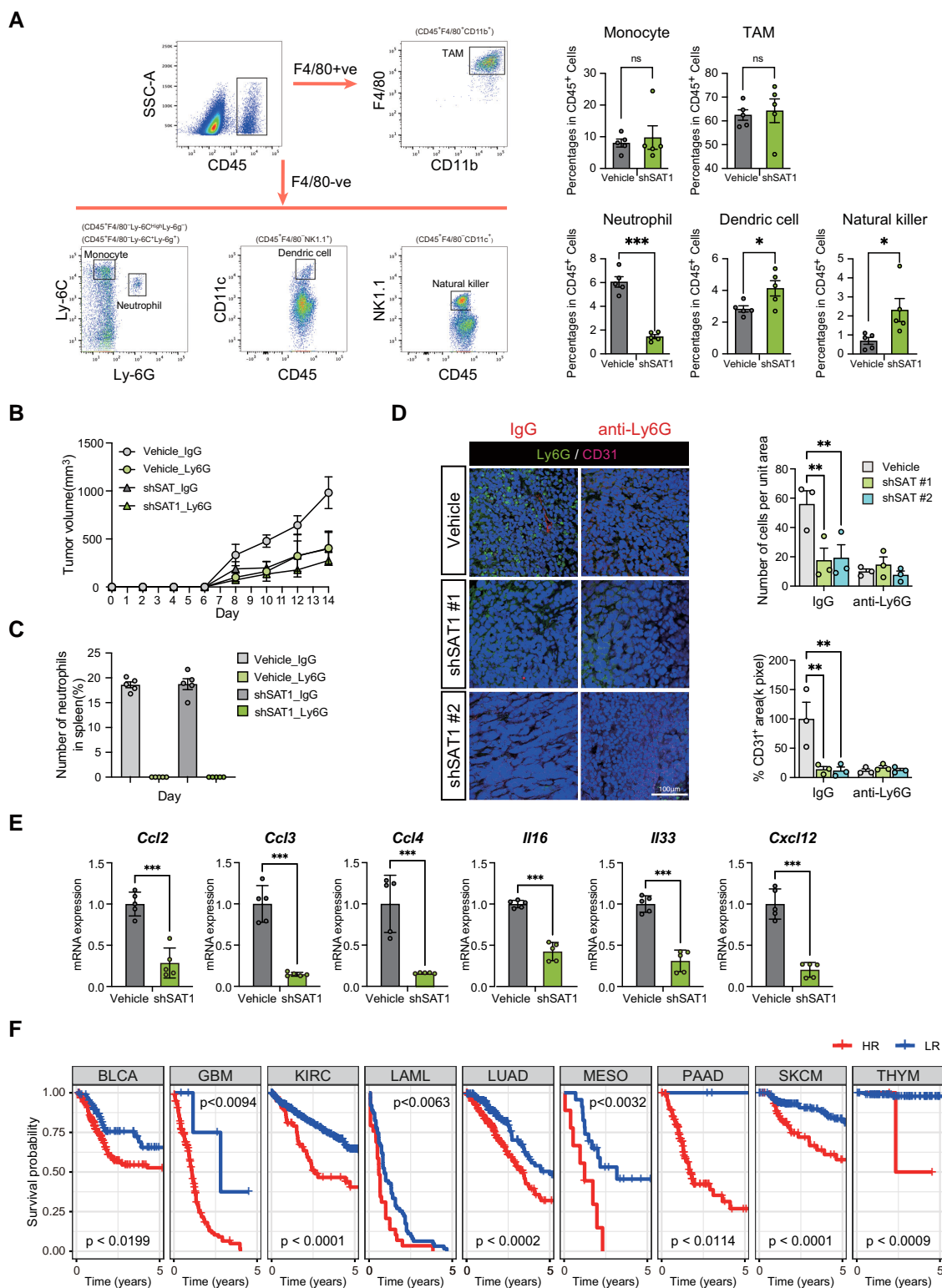


Fig. 4. SAT1-mediated recruitment of neutrophils stimulates tumor progression. **A**) Schematic showing experimental workflow for sorting CD45⁺ immune cells from tumor xenografts using fluorescence-activated cell sorting (FACS). Percentage of monocytes (CD45⁺ F4/80⁻ Ly6C^{high} Ly6G⁻), tumor-associated macrophages (CD45⁺ F4/80⁺ CD11b⁺), neutrophils (CD45⁺ F4/80⁺ Ly6C⁺ Ly6G⁺), dendritic cells (CD45⁺ F4/80⁻ CD11c⁺), and NK cells (CD45⁺ F4/80⁻ NK1.1⁺) in CD45⁺ immune cells are shown for tumors of human cancer (HeLa) xenograft under sh-control or shSAT1 treatment (right). **B**) Tumor growth in the shSAT1 human cancer (HeLa) xenograft model with anti-IgG or antineutrophil (anti-Ly6G) antibody treatment. **C**) Numbers of neutrophils in spleen of the shSAT1 human cancer (HeLa) xenograft model with anti-IgG or anti-Ly6G treatment at day 14. **D**) Immunostaining of the shSAT1 human cancer (HeLa) xenograft model with anti-IgG or anti-Ly6G treatment. Neutrophils, endothelial cells, and nuclei are indicated by Ly6G, CD31, and DAPI, respectively. Scale bars: 100 μ m (left). Numbers of Ly6G⁺ neutrophils per unit area and percentage of CD31⁺ area in tumor xenograft (right). **E**) mRNA expression of cytokines (*Ccl2*, *Ccl3*, *Ccl4*, *Il16*, *Il33*, and *Cxcl12*) in vehicle- or shSAT1-treated tumor of human cancer (HeLa) xenograft. **F**) Kaplan–Meier plots for estimation of overall survival of patients. Patients were classified into high risk (HR) and low risk (LR) using the Lasso-regularized Cox proportional hazard model based on expression profiles of genes with reduced expression following shSAT1 treatment. Data represent the mean \pm SEM of at least three independent experiments. NS: not significant; **P* < 0.05; ***P* < 0.01; ****P* < 0.001.

suggesting that modulation of NK cell and/or neutrophil behavior via SAT1 influences tumor progression.

To investigate whether the effect of shSAT1 on decreased tumor volume was due to NK cells or neutrophils, we first examined if inhibition of NK cells increased tumor growth in shSAT1 knockdown tumors. Although the number of NK cells was significantly lower in spleens following this intervention, depletion of NK cells by anti-asialo-GM1 antibody did not affect the growth of shRNA knockdown tumors (Fig. S6A and B). We confirmed that shSAT1 decreased the number of neutrophils in tumor by immunofluorescence (Fig. S6C). We next hypothesized that lower neutrophil numbers following SAT1 knockdown may decrease tumor growth. We examined whether depletion of neutrophils suppresses tumor growth in vehicle-treated shRNA control tumors to a similar extent to that seen in shSAT1 tumors. Anti-Ly6G antibody treatment significantly decreased the number of neutrophils in shRNA control tumors, to a similar extent to that seen in SAT1 knockdown tumors and suppressed tumor growth of control shRNA. In contrast, the antibody treatment did not significantly affect tumor growth in shSAT1 tumors when compared to growth seen under isotype-matched control antibody treatment (Fig. 4B); as expected, the number of neutrophils was significantly lower in spleens following this intervention (Fig. 4C). In addition, anti-Ly6G antibody significantly decreased neutrophil infiltration and angiogenesis in control tumors (Fig. 4D), suggesting that the SAT1-N1-acetylspermidine axis decreased neutrophil numbers, contributing to decreased tumor growth.

To further examine the role of the SAT1-N1-acetylspermidine axis, we examined expression levels of inflammatory cytokines in vehicle- or shSAT1-treated tumors (Fig. S6D and E). mRNA expression levels of *Ccl2*, *Ccl3*, *Ccl4*, *Il16*, *Il33*, and *Cxcl12* were significantly decreased following shSAT1 treatment (Fig. 4E), suggesting that the SAT1-N1-acetylspermidine axis stimulates expression of inflammatory cytokines promoting infiltration of neutrophils into tumors. To investigate the effect of N1-acetylspermidine on neutrophil migration, we performed a trans-well migration assay on human neutrophil-like cell line HL-60. We found that the addition of N1-acetylspermidine to the cell culture increases the cell migration ability of HL-60 (Fig. S6F), altogether suggesting that acidic pH-induced N1-acetylspermidine from cancer cells promotes tumor growth via protumorigenic neutrophil infiltration.

We hypothesized that SAT1 may contribute to cancer progression and decrease overall survival in patients. We performed a Kaplan–Meier survival analysis for genes down-regulated by shSAT1 (Table S5) and found that there was markedly reduced overall survival in patients with bladder urothelial carcinoma (BLCA), glioblastoma multiforme (GBM), kidney renal clear cell carcinoma (KIRC), acute myeloid leukemia (LAML), lung adenocarcinoma (LUAD), mesothelioma (MESO), pancreatic adenocarcinoma (PAAD), skin cutaneous melanoma (SKCM), and thymoma (THYM) (Fig. 4F; Table S6), indicating the importance of SAT1 in cancer progression and malignancy. The role of SAT1, however, may vary across different cell types, which could have implications for the proposed therapeutic strategies.

Discussion

In this study, using comprehensive metabolomic analyses, we demonstrated that acidic pH induces changes in the polyamine metabolic pathway through up-regulation of SAT1 expression, resulting in accumulation of N1-acetyl spermidine, via a protumorigenic metabolic pathway distinct from those characteristic of hypoxia and nutrient starvation. The SAT1-N1-acetylspermidine axis stimulated *in vivo* tumor growth accompanied by infiltration

of protumor neutrophils, suggesting that this axis can act as a protumorigenic immunomodulator.

Tumor microenvironments such as those characterized by hypoxia and nutrient starvation contribute to tumor malignancy (22). In tumor microenvironments, the pH can become as acidic as pH 6.4–6.9 due to elevated glycolysis and proton and lactate secretion under hypoxia (23, 24); however, the metabolic reprogramming associated with acidic pH has remained largely unknown. We found that acidic pH induces metabolic alteration of polyamine pathways through up-regulation of SAT1, a rate-limiting enzyme, with the changes being different from those induced by hypoxia and nutrient starvation, suggesting the existence of acidic pH-responsive metabolic regulation distinct from those of hypoxia and nutrient starvation. We found that the polyamine pathway is involved in a major metabolic response to acidic pH, distinct from pathways identified for hypoxic responses (e.g. glycolysis) and nutrient starvation (e.g. amino acid metabolism) and contributing to the metastatic phenotypes of a variety of cancer types (7–10).

Polyamine metabolism has been reported to be regulated in highly metastatic cancers, such as castration-resistant prostate cancer (7), colon cancer (8), medulloblastoma (9), and BRAF mutant melanoma (10). SAT1 is a rate-limiting enzyme in polyamine metabolism (25, 26) and has been shown to directly regulate transcription (27); however, its involvement in cancer progression has not been well understood.

We found that SAT1 activity led to accumulation of N1-acetylspermidine under conditions of acidic extracellular pH (pH 6.8) and stimulated protumor neutrophil infiltration into tumors, consistent with a recent report (12) that polyamines can modulate tumor immunity. In addition, we found that lactic acidification, as opposed to lower pH achieved at lower NaHCO_3 levels, triggered up-regulation of SAT1 expression and accumulation of N1-acetylspermidine, indicating that activation of SAT1 was not a specific response to low NaHCO_3 levels.

SAT1 has previously been reported to be associated with the adaptive immune system in the TME, including with CD8^+ T cells (28). Additionally, we have recently reported that spermidine suppresses the proliferation of CD8^+ T cells in the syngeneic tumor model (29). We found that SAT1 knockdown did not lead to the accumulation of spermidine (Fig. S4C); therefore, CD8^+ T cell activation is not responsible for the reduced tumor volume in the SAT1 KD tumor in the mouse model. To explore other possible mechanisms linking SAT1 in cancer to the TME, in this study, we focused on the up-regulation of SAT1 expression in cancer cells under acidic pH and the effect of the resulting metabolite, N1-acetylspermidine, on protumor immunity.

CD11b^+ myeloid cells have been considered important components in protumor immunity for their roles in matrix remodeling and secretion of proinflammatory cytokines (30). Furthermore, CD11b^+ myeloid cells were reported to promote the suppression of T cell proliferation and are associated with the absence of $\text{IFN-}\gamma$ response in the tumor microenvironment during the early stages of oncolytic virus therapy (31). Thus, CD11b^+ myeloid cells are recently gaining attention as indicators of tumorigenicity and potent immunotherapeutic targets.

Extensive studies have reported neutrophil heterogeneity and specific markers for protumor neutrophils (32, 33). However, in this study, we did not differentiate neutrophils based on specific subtypes (we used a marker for Ly6G^+ neutrophils). We found that depletion of neutrophils with anti-Ly6G significantly suppresses tumor progression and concluded that anti-Ly6G targeted the protumor neutrophil.

In conclusion, our findings provide evidence that the SAT1-N1-acetylspermidine axis plays an important role in immunomodulation and tumor progression in response to extracellular acidification. An important goal for future studies will be to understand the mechanisms by which acidic intracellular pH activates SAT1 in cancer cells. Based on the results of the present study, we suggest that inhibitors of SAT1-N1-acetylspermidine-mediated immunomodulation may prove to be effective chemotherapeutic agents in combination with conventional chemotherapy, offering a therapeutic approach to treating acidosis-activated malignant cancers.

Materials and methods

Acidic pH cell culture

Human epithelial cell line derived from pancreatic cancer PANC-1, human pancreatic cell line derived from adenocarcinoma ascites AsPC-1, human cervical cancer cell line HeLa, human epidermoid carcinoma A431, human colorectal carcinoma cell lines HCT116, and human neutrophil-like cell line HL-60 were purchased from the American Type Culture Collection (ATCC). AsPC-1, HeLa, A431, and HCT116 were maintained in Dulbecco's modified Eagle's medium (DMEM) (Nacalai Tesque) supplemented with 10% fetal bovine serum (FBS). PANC-1 and HL-60 were maintained in RPMI 1640 medium (Nacalai Tesque) supplemented with 10% FBS. All cells were maintained at 37°C in a 5% CO₂ atmosphere, except otherwise specified. Acidic pH culture (pH 6.8) was prepared by reducing the amount of NaHCO₃ or addition of lactate or hydrochloric acid (HCl) based on DMEM (Nissui). Cells were treated for 24 h under each condition, unless stated otherwise.

Metabolite extraction and metabolomic analysis

Metabolites extracted from cancer cell and tumor tissue samples were measured by CE-MS (Agilent Technologies). For the measurement of cationic metabolites, a fused silica capillary (50 mm i.d. × 100 cm) was used with the electrolyte 1 M formic acid. Methanol/water (50% v/v) containing 0.1 mM hexakis (2,2-difluoroethoxy) phosphazene was added at 10 μL/min as sheath solution. In positive ion mode, electrospray ionization (ESI)-TOFMS was performed and capillary voltage was set to 4 kV. Acquired spectrum recalibration was conducted by two reference standards ([¹³C isotopic ion of a protonated methanol dimer (2 MeOH + H)⁺, m/z 66.0632) and ([hexakis(2,2-difluoroethoxy)phosphazene + H]⁺, m/z 622.0290). To identify metabolites, relative migration times of all peaks were measured with normalization to the reference compound 3-aminopyrrolidine, comparing their m/z values and relative migration times to the standards. Quantification of metabolite level was performed by comparing peak areas of each metabolite to calibration curves generated using internal standardization with methionine sulfone. Measurement of cationic metabolites, a commercially available COSMO(+) (chemically coated with cationic polymer) capillary (50 mm i.d. × 105 cm), was used with a 50 mM ammonium acetate solution (pH 8.5) as the electrolyte. Methanol/5 mM ammonium acetate (50% v/v) containing 0.1 mM hexakis (2,2-difluoroethoxy) phosphazene was applied at 10 mL/min as the sheath liquid. ESI-TOFMS was performed in negative ion mode, and the capillary voltage was set to 3.5 kV. Trimesate and CAS were used for the reference of the internal standards. Capillary electrophoresis time-of-flight mass spectrometry (CE-TOFMS) raw data were analyzed using Master Hands software (Ver. 2.17.0.10). Relative peak areas were calculated by the ratio of peak area divided by the internal standards. Metabolite

concentrations were calculated based on the relative peak area between the sample and the standard as previously described (18, 34)

RNA-seq data analysis

RNA-seq data were aligned to the human transcriptome (UCSC gene) and genome (GRCh37/hg19) references respectively by using Burrows–Wheeler Aligner software package. After transcript coordinate was converted to genomic positions, an optimal mapping result was chosen from either transcript or genome mapping according to minimal distance to the reference. Local realignment was completed within in-house short reads aligner with a smaller k-mer size (k = 11). Fragments per kilobase of exon per million fragment mapped (FPKM) values were calculated for each UCSC gene for strand-specific information as previously described (18)

Quantitative real-time PCR

The total RNA of cells was extracted using Isogen reagent (Nippon Gene) and converted to cDNA by applying the PrimeScript reverse transcriptase (Takara) as per the manufacturer's instructions. Converted cDNA was used for quantitative real-time PCR amplification with Thunderbird SYBR Green qPCR mix (Toyobo) and primers (Table S4). All results of mRNA expression level were normalized by the expression level of ACTB.

Western blotting

Aliquots of proteins were separated by SDS–PAGE and transferred to nitrocellulose membrane (BioRad Laboratories). Immunodetection was carried out with Rabbit polyclonal anti-SAT1 (ProteinTech, #10708-1-AP, 1:200), rabbit polyclonal anti-PAOX (ProteinTech, #18972-1-AP, 1:3,000), rabbit polyclonal anti-SRM (19858-1-AP, ProteinTech, 1:1,500), and mouse monoclonal anti-β-actin (Sigma-Aldrich #A5441, 1:5,000): antibodies in combination with peroxidase-conjugated affinity-purified donkey antimouse (Sigma-Aldrich, 1:1,000) or antirabbit (Cell Signaling Technology, 1:1,000) IgG and then visualized using SuperSignal™ West Dura Extended Duration Substrate (Thermo Fisher Scientific). Luminescence images were analyzed by luminescent image analyzer (Fusion FX, Vilber).

Overexpression of SAT1

For transient overexpression of SAT1, PANC-1 or HeLa cells were transfected with the corresponding plasmid using Lipofectamine 2000 (Invitrogen). Cells at 70% confluence were incubated for 24 h with 20 μL of Lipofectamine 2000 and 8 μg of plasmid DNA. DNA–lipid complexes were diluted in Opti-Minimal Essential Medium (Opti-MEM; Gibco) and incubated for 30 min before being added to the cells. After 24 h of transfection, the medium was changed to a medium containing serum. Expression level of mRNA and metabolite level of cells were analyzed 48 h after transfection.

Gene silencing using siRNA or shRNA

siRNAs designed against human SAT1 were obtained commercially (Thermo Fisher Scientific). In this study, two sequences of siRNAs were used against SAT1, designated as siRNA:

sense: 5'-CCUUGAAUAUCUUUCGAUAaa-3' and antisense: 5'-UAUCGAAAGAUUAUCAAGGag-3';

siRNA2:

sense: 5'-UAUCGAAAGAUUAUCAAGGag-3' and antisense: 5'-UAGCAAGUACUCCUUGUCGat-3', respectively.

Cells were transfected with siRNAs against target genes or negative (scramble) control siRNA using Lipofectamine RNAiMAX transfection reagent (Thermo Fisher Scientific) according to the instructions of the manufacturer. In addition, two sequences of shRNAs were used against SAT1, designated as

shRNA1:

sense: 5'-ccggCCTTGAATATCTTTTCGATAAAActcgagTTTATCGAAAGATATCAAGGtttttg-3' and antisense: 5'-aattcaaaaaCCTTGAAATATCTTTTCGATAAAActcgagTTTATCGAAAGATATCAAGG-3'

shRNA2:

sense: 5'-aattcaaaaaCCTTGAATATCTTTTCGATAAAActcgagTTTATCGAAAGATATCAAGG-3' and antisense 5'-aattcaaaaaCGACAAGGAGTACTTGCTAAActcgagTTTAGCAAGTACTCCTTGTCG-3', respectively. shRNAs expressing 293 T cells was generated for lentiviral infection, and shRNA expressing target cells were selected with puromycin. The ability of the si/shRNA to inhibit target gene expression was assessed posttransfection.

Animal studies and tumor xenograft

PANC-1 or HeLa cells (1×10^7) were subcutaneously injected into C.B17/Icr-scidJcl scid/scid mice. Tumor volume was measured every other day and analyzed using the paired Student's *t*-test. All animal care procedures were in accordance with institutional guidelines approved by The University of Tokyo.

Immunohistochemical staining

Tumors were isolated, directly embedded in optimal cutting temperature (OCT) compound and stored in -80°C until analysis. Frozen tumor tissues were cut 15- μm thick by using Cryostat CM1950 (Leica), fixed with 4% paraformaldehyde, and stained with Hamster monoclonal antimouse PECAM-1 (Sigma-Aldrich, Cat# MAB1398Z; 1:100), rat monoclonal antimouse CD11b (BD Pharmingen, Cat# 550282; 1:100), and rat monoclonal antimouse Ly6G (BioLegend, Cat# 127602; 1:100) primary antibodies for overnight at 4°C . The sections were then incubated for 60 min at room temperature with Alexa Fluor 488-conjugated goat antirat (Thermo Fisher Scientific), Alexa Fluor 568-conjugated goat antimouse (Thermo Fisher Scientific), or Alexa Fluor 568-conjugated goat antirabbit (Thermo Fisher Scientific) secondary antibodies, which were diluted at 1:1,000 in phosphate buffered saline (PBS). Tumor sections were mounted on Dapi-Fluoromount-G (SouthernBiotech) and then analyzed using a confocal microscope (STELLARIS 5, Leica).

Gene expression analysis of mouse immune cell populations

To examine the immune cell population in each sample, the expression of mouse genes was quantified through RNA-seq. The process entailed aligning RNA-seq reads to the GRCh38 human genome reference and then diverting unmapped reads to the mouse genome (mm10) reference using STAR version 2.7.10a (35). Utilizing the derived bam files, HTseq version 2.0.2 (36) was employed to generate a gene-wise count matrix. The composition of immune cell types was analyzed using quanTIseq (37) in the R package immunedeconv (version 2.1.0) (38) with default parameters and an input signature matrix.

Violin plots of the differences in the percentage of cell types identified by quanTIseq in shSAT1 samples and control samples are shown in Fig. 3F.

We then employed the R package DESeq2 (version 1.38.0) (39) to identify differentially expressed genes between shSAT1 samples and control samples.

The genes that were up-regulated and down-regulated in shSAT1 samples compared to control samples were identified using the following criteria. The down-regulated genes of the shSAT1 samples were 73 genes that satisfied the following criteria: (i) the log₂-fold change (shSAT1 vs control) was $\leq \log_2(1/1.2)$, and (ii) the *P*-value of DESeq2 (shSAT1 vs control) was ≤ 0.05 .

Flow cytometry analysis

Tumor xenografts were isolated from mice, excised, minced, and treated by collagenase (0.75 $\mu\text{g}/\text{mL}$, Roche), DNase I (40 $\mu\text{g}/\text{mL}$, Roche), and dispase (0.5 $\mu\text{g}/\text{mL}$, Thermo Fisher Scientific), with rigorous agitation (180 rpm, 37°C , 1 h). The resulting cell suspension was passed through cell strainer (BD Falcon) and treated with RBC lysis buffer (Invitrogen). After washing by PBS, cells were incubated with anti-CD16/32 antibody (BioLegend) for 5 min on ice. The following antibodies were purchased from BioLegend and used: APC or PerCP-Cy5.5 anti-CD11b mAb (M1/70); PE anti-Ly6C mAb (HK1.4); APC anti-CD11c mAb (N418); FITC anti-NK1.1 mAb (PK136); APC anti-CD206 mAb (C068C2); FITC anti-F4/80 mAb (BM8); Pacific Blue anti-Ly6G mAb (1A8); and Pacific Blue or APC-Cy7 anti-CD45 mAb (IM7). The cells were then stained with antibodies in PFE (PBS with 2% FBS and 1 mM of EDTA) for 20 min on ice and analyzed by BD LSR Fortessa (BD Biosciences). Flow cytometry data were collected by FACSDiva (BD Biosciences). Collected data were analyzed with FlowJo software (v10.2, BD Biosciences).

Migration assay of HL-60

10^6 neutrophil (HL-60) cells were seeded on the upper chamber of 8- μm pore Transwell plate (Corning) in 200 μL of RPMI 1640 supplemented with 1% FBS. In the lower chamber, 500- μL RPMI 1640 supplemented with 10% FBS was added. Cells were cultured for 8 h under with/without 100 μM N1-acetylspermidine, and the number of migrated cells in the lower chamber was counted by TC20 Automatic Cell Counter (BioRad).

Survival analysis

To evaluate prognosis of cancer patients by differential expression profiles of genes in shSAT1 cells, we analyzed RNA-seq expression data from following 30 cancer cohorts (49 adrenocortical carcinoma [ACC], 330 BLCA, 1,073 breast invasive carcinoma [BRCA], 236 cervical squamous cell carcinoma and endocervical adenocarcinoma [CESC], 25 cholangiocarcinoma [CHOL], 161 colon adenocarcinoma [COAD], 45 lymphoid neoplasm diffuse large B-cell lymphoma (DLBC), 147 esophageal carcinoma (ESCA), 163 GBM, 465 head and neck squamous cell carcinoma [HNSC], 84 kidney chromophobe [KICH], 595 KIRC, 286 kidney renal papillary cell carcinoma [KIRP], 92 LAML, 481 brain lower grade glioma [LGG], 365 liver hepatocellular carcinoma [LIHC], 490 LUAD, 468 lung squamous cell carcinoma [LUSC], 32 MESO, 302 ovarian serous cystadenocarcinoma [OV], 152 PAAD, 483 prostate adenocarcinoma [PRAD], 52 rectum adenocarcinoma [READ], 208 SARC, 290 SKCM, 344 stomach adenocarcinoma [STAD], 521 thyroid carcinoma [THCA], 115 THYM, 376 Uterine Corpus Endometrial Carcinoma [UCEC], and 21 uterine carcinosarcoma [UCS]) from the Broad TCGA GDAC web site (<http://gdac.broadinstitute.org/>).

To build a SAT1 signature-based prognostic classifier, we utilized a Lasso-regularized Cox proportional hazard model using the glmnet package (version 4.1.2) in R statistical environment (version 4.2.2). The tuning parameter λ in the Lasso regularization was chosen based on the corrected Akaike's information criterion. The Cox model for each cohort is summarized in Table S6. Out of the 30 cohorts, 21 studies (ACC, BRCA, CESC, CHOL, COAD, DLBC, ESCA, HNSC, KICH, KIRP, LGG, LIHC, LUSC, OV, PRAD, READ, SARC, STAD,

THCA, UCEC, and UCS) were not used for further analysis. For the remaining nine cohorts (BLCA, GBM, KIRC, LAML, LUAD, MESO, PAAD, SKCM, and THYM), patients were classified into two groups based on their risk score in the Cox model. The prognostic significance of the Cox model was evaluated by Kaplan–Meier method, and log-rank test was used in the calculation of the P-values, which were further corrected for multiple hypothesis testing using the Benjamini–Hochberg procedure as previously described (18).

Acknowledgments

We thank the members of the Division of Nutriomics and Oncology, Laboratory for Systems Biology and Medicine, Genome Science and Medicine, the RCAST, University of Tokyo. We especially thank Dr. T. Tanaka, Dr. H. Aburatani, and Ms. K. Shiina for their helpful discussions and support.

Supplementary Material

Supplementary material is available at PNAS Nexus online.

Funding

This work was supported by Grant-in-Aid for Scientific Research (B) (19H03496, T.O.), Grant-in-Aid for Scientific Research on Innovative Areas (20H04834, T.O.), Grant-in-Aid for challenging Exploratory Research (19K22553, 21K19399, and 23K18234, T.O.), JSPS KAKENHI Grant AdAMS (22H04922), Grant-in-Aid for Scientific Research (S) (JP23H05473, M.Y.), and Grant-in-Aid for JSPS Fellows Grant Numbers 22J13979, 23KJ0581(K.M., R.N.) from the Ministry of Education, Culture, Sports, Science, and Technology of Japan and also supported by Leadership Development Program for PhD (LDPP) by the University of Tokyo (K.M.), partly supported by Extramural Collaborative Research Grant of Cancer Research Institute, Kanazawa University and Nanken-Kyoten (Grant No. 2023-kokunai 34) TMDU, the Sumitomo Foundation (T.O.), The Shimadzu Science Foundation (T.O.), the Kurata Grant (T.O.), the Naito Foundation (T.O.), the Uehara Memorial Foundation (T.O.), the SGH Foundation (T.O.), the Koyanagi Foundation (T.O.), The Takeda Foundation (S.A. and T.O.), and the Project for Promotion of Cancer Research and Therapeutic Evolution (P-PROMOTE), from Japan Agency for Medical Research and Development, AMED (T.O.).

Author contributions

T.O. designed research; M.K., K.M., R.N., A.K., S.A., M.S., M.N., M.H., H.M., S.H., H.Y., and T.O. performed research; M.K., K.M., H.H., S.A., R.A., R.T., M.Y., M.Y., T.T., T.K., H.Y., T.S., and T.O. analyzed and interpreted data; and M.K., R.N., and T.O. wrote the paper.

Data availability

All data required for the main findings of this manuscript are included in the article and supplemental materials except result of RNA-sequencing. RNA-sequencing result related to Fig. 3D–F is available in Gene Expression Omnibus (GEO) under the accession number GSE239784.

References

- Pranzini E, Pardella E, Paoli P, Fendt S-M, Taddei ML. 2021. Metabolic reprogramming in anticancer drug resistance: a focus on amino acids. *Trends Cancer*. 7(8):682–699.
- Faubert B, Solmonson A, DeBerardinis RJ. 2020. Metabolic reprogramming and cancer progression. *Science* 368(6487):eaaw5473. <https://doi.org/10.1126/science.aaw5473>
- Warburg O. 1956. On the origin of cancer cells. *Science* 123(3191):309–314.
- Barker J, Khan M, Solomos T. 1964. Mechanism of the Pasteur effect. *Nature* 201(4924):1126–1127.
- Corbet C, Feron O. 2017. Tumour acidosis: from the passenger to the driver's Seat. *Nat Rev Cancer*. 17(10):577–593.
- Kondo A, et al. 2017. Extracellular acidic pH activates the sterol regulatory element-binding protein 2 to promote tumor progression. *Cell Rep*. 18(9):2228–2242.
- Zabala-Letona A, et al. 2017. mTORC1-dependent AMD1 regulation sustains polyamine metabolism in prostate cancer. *Nature* 547(7661):109–113.
- Roy UK, Rial NS, Kachel KL, Gerner EW. 2008. Activated K-ras increases polyamine uptake in human colon cancer cells through modulation of caveolar endocytosis. *Mol Carcinog*. 47(7):538–553.
- D'Amico D, et al. 2015. Non-canonical hedgehog/AMPK-mediated control of polyamine metabolism supports neuronal and medulloblastoma cell growth. *Dev Cell*. 35(1):21–35.
- Peters M, Minton A, Phanstiel IV O, Gilmour S. 2018. A novel polyamine-targeted therapy for BRAF mutant melanoma tumors. *Med Sci (Basel)*. 6(1):3.
- Tabib A, Bachrach U. 1998. Polyamines induce malignant transformation in cultured NIH 3T3 fibroblasts. *Int J Biochem Cell Biol*. 30(1):135–146.
- Al-Habsi M, et al. 2022. Spermidine activates mitochondrial trifunctional protein and improves antitumor immunity in mice. *Science* 378:6618. <https://doi.org/10.1126/science.abj3510>
- Yang M, Soga T, Pollard PJ. 2013. Oncometabolites: linking altered metabolism with cancer. *J Clin Invest*. 123(9):3652–3658.
- Intlekofer AM, et al. 2015. Hypoxia induces production of L-2-hydroxyglutarate. *Cell Metab*. 22(2):304–311.
- Intlekofer AM, et al. 2017. L-2-Hydroxyglutarate production arises from noncanonical enzyme function at acidic pH. *Nat Chem Biol*. 13(5):494–500.
- Xu W, et al. 2011. Oncometabolite 2-hydroxyglutarate is a competitive inhibitor of α -ketoglutarate-dependent dioxygenases. *Cancer Cell* 19(1):17–30.
- Adam J, et al. 2011. Renal cyst formation in FH1-deficient mice is independent of the HIF/PhD pathway: roles for fumarate in keap1 succination and Nrf2 signaling. *Cancer Cell* 20(4):524–537.
- Osawa T, et al. 2019. Phosphoethanolamine accumulation protects cancer cells under glutamine starvation through downregulation of PCYT2. *Cell Rep*. 29(1):89–103.e7. <https://doi.org/10.1016/j.celrep.2019.08.087>
- Pollard PJ, et al. 2005. Accumulation of krebs cycle intermediates and over-expression of hif1 α in tumours which result from germline FH and SDH mutations. *Hum Mol Genet*. 14(15):2231–2239.
- Gimenez-Roqueplo A-P, et al. 2002. Functional consequences of *asdhb* gene mutation in an apparently sporadic pheochromocytoma. *J Clin Endocrinol Metab*. 87(10):4771–4774.
- Xiao M, et al. 2012. Inhibition of α -kg-dependent histone and DNA demethylases by fumarate and succinate that are accumulated in mutations of FH and SDH tumor suppressors. *Genes Dev*. 26(12):1326–1338.
- Tredan O, Galmarini CM, Patel K, Tannock IF. 2007. Drug resistance and the solid tumor microenvironment. *J Natl Cancer Inst*. 99(19):1441–1454.
- Gerweck LE, Seetharaman K. 1996. Cellular pH gradient in tumor versus normal tissue: potential exploitation for the treatment of cancer. *Cancer Res*. 56(6):1194–1198.

- 24 Webb BA, Chimenti M, Jacobson MP, Barber DL. 2011. Dysregulated PH: a perfect storm for cancer progression. *Nat Rev Cancer*. 11(9): 671–677.
- 25 Kramer DL, et al. 2008. Polyamine acetylation modulates polyamine metabolic flux, a prelude to broader metabolic consequences. *J Biol Chem*. 283(7):4241–4251.
- 26 Pegg AE. 2008. Spermidine/spermine-N1-acetyltransferase: a key metabolic regulator. *Am J Physiol Endocrinol Metab*. 294(6):E995–E1010.
- 27 Thakur VS, Aguila B, Brett-Morris A, Creighton CJ, Welford SM. 2019. Spermidine/spermine N1-acetyltransferase 1 is a gene-specific transcriptional regulator that drives brain tumor aggressiveness. *Oncogene* 38(41):6794–6800.
- 28 Mou Y, Zhang L, Liu Z, Song X. 2022. Abundant expression of ferroptosis-related SAT1 is related to unfavorable outcome and immune cell infiltration in low-grade glioma. *BMC Cancer* 22(1): 215. <https://doi.org/10.1186/s12885-022-09313-w>
- 29 Hibino S, et al. 2023. Tumor cell-derived spermidine is an oncometabolite that suppresses TCR clustering for intratumoral CD8⁺ T cell activation. *Proc Natl Acad Sci U S A*. 120(24): e2305245120. <https://doi.org/10.1073/pnas.2305245120>
- 30 Yan HH, et al. 2010. GR-1⁺ CD11b⁺ myeloid cells tip the balance of immune protection to tumor promotion in the premetastatic lung. *Cancer Res*. 70(15):6139–6149.
- 31 Clements DR, et al. 2015. Newly recruited cd11b⁺, GR-1⁺, ly6chigh myeloid cells augment tumor-associated immunosuppression immediately following the therapeutic administration of oncolytic reovirus. *J Immunol*. 194(9):4397–4412.
- 32 Kowanetz M, et al. 2010. Granulocyte-colony stimulating factor promotes lung metastasis through mobilization of ly6g⁺ ly6c⁺ granulocytes. *Proc Natl Acad Sci U S A*. 107(50): 21248–21255.
- 33 Jaillon S, et al. 2020. Neutrophil diversity and plasticity in tumour progression and therapy. *Nat Rev Cancer*. 20(9):485–503.
- 34 Pan M, et al. 2022. Glutamine deficiency in solid tumor cells confers resistance to ribosomal RNA synthesis inhibitors. *Nat Commun*. 13(1):3706.
- 35 Alexander D, et al. 2013. STAR: ultrafast universal RNA-seq aligner. *Bioinformatics* 29(1):15–21.
- 36 Putri G, et al. 2022. Analysing high-throughput sequencing data in Python with HTSeq 2.0. *Bioinformatics* 38(10):2943–2945.
- 37 Finotello F, et al. 2019. Molecular and pharmacological modulators of the tumor immune contexture revealed by deconvolution of RNA-seq data. *Genome Med*. 11(1):34.
- 38 Sturm G, Finotello F, List M. 2022. Immunedeconv: an R package for unified access to computational methods for estimating immune cell fractions from Bulk RNA-sequencing data. *Methods Mol Biol*. 2120:223–232.
- 39 Love MI, Huber W, Anders S. 2014. Moderated estimation of fold change and dispersion for RNA-seq data with DESeq2. *Genome Biol*. 15(12):550.